Supplementary Information for: **Imaging breast cancer using hyperpolarized carbon-13 MRI**

Ferdia A. Gallagher[a,b,c,1], Ramona Woitek[a,c,d,1,2], Mary A. McLean[a,c,e], Andrew B. Gill[a], Raquel Manzano Garcia[c,e], Elena Provenzano[c,f,g] , Frank Riemer[a], Joshua Kaggie[a], Anita Chhabra[h], Stephan Ursprung[a,c], James T. Grist[a], Charlie J. Daniels[a], Fulvio Zaccagna[a], Marie-Christine Laurent[a], Matthew Locke[a], Sarah Hilborne[a], Amy Frary[a], Turid Torheim[c,e,], Chris Boursnell[c,e], Amy Schiller[b], Ilse Patterson[b], Rhys Slough[b], Bruno Carmo[b], Justine Kane[f], Heather Biggs[f], Emma Harrison[f], Surrin S Deen[a], Andrew Patterson[a,b], Titus Lanz[i], Zoya Kingsbury[j], Mark Ross[j], Bristi Basu[c,k], Richard Baird[f], David J. Lomas[a], Evis Sala[a,b,c], James Wason[l,m] , Oscar M Rueda[c,e], Suet-Feung Chin[c,e], Ian B. Wilkinson[n], Martin J. Graves[a,b], Jean E Abraham[c,f,k], Fiona J. Gilbert[a,b,c], Carlos Caldas[c,e,f,k], Kevin M. Brindle[c,e,o]

[1]F.A.G and R.W. contributed equally to this work.

[2]To whom correspondence may be addressed. Email: rw585@cam.ac.uk.

[a]Department of Radiology, University of Cambridge, Cambridge, CB2 0QQ, United Kingdom

[b]Department of Radiology, Addenbrooke's Hospital, Cambridge University Hospitals National Health Service Foundation Trust, Cambridge, CB2 0QQ, United Kingdom

[c]Cancer Research UK Cambridge Centre, University of Cambridge, Robinson Way, Cambridge, CB2 0RE, United Kingdom

[d]Department of Biomedical Imaging and Image-guided Therapy, Medical University of Vienna, 1090 Vienna, Austria

[e]Cancer Research UK Cambridge Institute, University of Cambridge, Cambridge, CB2 0RE, United Kingdom

[f]Cambridge Breast Cancer Research Unit, Addenbrooke's Hospital, Cambridge University Hospital National Health Service Foundation Trust, Cambridge, CB2 0QQ, United Kingdom

[g]Department of Histopathology, Addenbrooke's Hospital, Cambridge University Hospitals National Health Service Foundation Trust Cambridge, CB2 0QQ, United Kingdom

[h]Pharmacy Department, Cambridge University Hospitals National Health Service Foundation Trust, Cambridge, CB2 0QQ, United Kingdom

[i]RAPID Biomedical GmbH, 97222 Rimpar, Germany

[j]Illumina, Great Chesterford, CB10 1XL, United Kingdom

[k]Department of Oncology, University of Cambridge, Cambridge, CB2 0QQ, United Kingdom

[l]Medical Research Council Biostatistics Unit, University of Cambridge, Cambridge, CB2 0QQ, United Kingdom

[m]Institute of Health and Society, Newcastle University, Newcastle-upon-Tyne, NE2 4AX, United Kingdom

[n]Department of Experimental Medicine and Immunotherapeutics, University of Cambridge, Cambridge, CB2 0QQ, United Kingdom

[o]Department of Biochemistry, University of Cambridge, Cambridge, CB2 0QQ, United Kingdom

www.pnas.org/cgi/doi/10.1073/pnas.1913841117

This PDF file includes:

Supplementary Information

Methods

Proton MRI. Sequence specifications for T1-weighted axial and coronal 3D fast spoiled gradient echo images used to plan the ^{13}C-MRI: FOV = 35 cm; matrix = 256 x 256; TE = 2.1 ms; TR = 5.292 ms; flip angle = 10°; slice thickness = 2.8 mm.

Sequence specifications for dynamic contrast enhanced (DCE) MRI (volume image breast assessment–time resolved imaging of contrast kinetics, VIBRANT-TRICKS): FOV = 350 mm; matrix = 512 x 512; reconstructed using an in-plane voxel size of 0.68 x 0.68 mm; slice thickness = 1.4mm; spectral-spatial water excitation; repetition time (TR) = 7.1 ms; echo time (TE) = 3.8 ms; flip angle (FA) = 12°).

Postprocessing of DCE MRI data: $T1_0$ maps were used to convert from signal intensity to gadolinium concentration. $T1_0$ mapping was based on a 3D variable flip angle (VFA) gradient echo method using FAs of 2°, 3°, 5°, 10°, and 15° used with an axial three-dimensional fast spoiled gradient-echo sequence (field of view, FOV = 350 mm; matrix = 256 x 256; interpolated slice thickness = 1.4 mm; in-plane voxel size = 0.6 x 0.6 mm²; TR = 5.3 ms; TE = 2.1 ms) (1). $T1_0$ maps were calculated using MIStar (Apollo Medical Imaging, Melbourne, Australia). RF transmit uniformity (B_1^+) maps were obtained using a multi-slice 2D Bloch-Siegert–based gradient-echo sequence (2) with the images postprocessed using in-house code (MATLAB, The MathWorks, Inc., Natick, MA); FOV = 350 mm; matrix = 128 x 128; slice thickness = 7 mm; in-plane voxel size = 2.7 x 2.7 mm²; TR = 29 ms; TE = 13.5 ms; FA = 20°. Spatial registration of B_1^+ corrected $T1_0$ maps and DCE was adjusted manually where necessary.

^{13}C Magnetic Resonance Imaging (^{13}C-MRI) and postprocessing. Pharmacy kits: the [1-^{13}C]pyruvic acid containing formulation was sealed, by laser welding, in a vial within the pharmacy kit. After preparation, pharmacy kits were stored at -20°C (3, 4). Before hyperpolarization, the vial containing the frozen pyruvate/EPA formulation was loaded into a clinical hyperpolarizer and defrosted for one hour (SPINlab, Research Circle Technology, Niskayuna, NY). Formulation of the neutralizing buffer solution

comprised 19 mL sterile water with 17.5 mL NaOH/Tris/EDTA (2.4%, 4.03%, and 0.033% w/v respectively, (Royal Free Hospital, London, UK).

QC criteria for injections: pH 6.7-8.1; EPA concentration ≤ 3 μM; pyruvate concentration 220-280 mM; and temperature 25-37 °C. After QC, the solution was passed through a sterilizing filter (0.2 μm; PureFlo Disc Filter, ZenPure, Manassas, VA) before collection in a sterile syringe (Medrad, Warrendale, PA).

The FOV was centered over the breast tumor and two to three coronal slices were acquired depending on the size of the breast. ^{13}C imaging started between 0 and 30 s after the ^{13}C-pyruvate injection.

Kinetic fitting was also explored as an alternative to analysis of metabolite ratios in the summed time courses. A two-way kinetic model (5) was used to fit the evolution of pyruvate and lactate signals between the time of peak pyruvate signal and the end of the acquisition. The forward rate constant k_{PL} from this fit was compared between patients. As an estimate of the uncertainty in fitting of k_{PL}, we calculated the variance for each metabolite between the measured and fitted data over the time series. For example, the variance for lactate over the series of N time points, Var(L), is calculated from the measured and fitted lactate intensities (L_m and L_f) as:

$$\mathrm{Var}(L) = \frac{\sum_{i=1}^{N}\left(L_{m_i} - L_{f_i}\right)^2}{\sum_{i=1}^{N}\left(L_{m_i}\right)^2}$$

The variance of lactate and pyruvate were then summed and examined as a metric of fit uncertainty (**Supporting Figure S2B**).

Immunohistochemistry and quantification for MCT1 and MCT4. For antigen retrieval, sections were incubated with Tris EDTA (for MCT1 and MCT4)for 20 minutes or with the Leica enzyme pretreatment solution (Leica enzyme pretreatment kit, Germany). Endogenous peroxidase activity was quenched using 3-4% (v/v) hydrogen peroxide. The primary antibodies used were HPA003324 (Atlas Antibodies, Bromma, Sweden) at a dilution of 1:500 for MCT1 and HPA021451 (Atlas Antibodies, Bromma, Sweden) at a

dilution of 1:500 for MCT4.The sections were then incubated with Anti-rabbit Poly-HRP-IgG polymer (<25 μg/mL) containing 10% (v/v) animal serum in tris buffered saline /0.09% ProClin™ 950 again to localize mouse antigen. The complex was then visualized using 66 mM 3,3'-Diaminobenzidine tetrahydrochloride hydrate in a stabilizer solution and ≤0.1% (v/v) Hydrogen Peroxide. Leica DAB Enhancer was added to enhance staining. Cell nuclei were counterstained with <0.1% hematoxylin. Optical densities for weak, moderate and strong stains used for the automated quantitative analysis of scanned sections were: MCT1, 0.576, 0.593, 0.674; MCT4, 0.722, 0.819, 0.909.

RNA sequencing. RNA from frozen tumor tissue sections of six patients was extracted using the QIAGEN miRNeasy Mini Kit (QIAGEN, Venlo, Netherlands; Cat No: 217004). Briefly, tissue sections were lysed in 700 μL of QIAzol and 140 μL of chloroform was added to each sample before being transferred to a heavy phase lock tube (QIAGEN MaXtract, Venlo, Netherlands; Cat no: 129056). The samples were centrifuged at 12,000 g for 15 min at 4°C, following which the upper aquaous phase was added to a fresh tube and x1.5 volume of 100% ethanol was added. The mixture was transferred to a miRNeasy column and centrifuged at 8,000 g for 1 min. The column was washed once with 700 μl RWT buffer followed by two 500 μl washes with RPE buffer. RNA was eluted into a clean tube with 50 μl RNAse free water.

Postprocessing of RNA sequencing data. To estimate gene counts we employed Salmon version 0.11.3 on read-based mode (6). The final estimated number of reads mapping to each gene was then normalized in three post-processing steps. First, we applied the edgeR package to estimate effective library sizes that account for sequencing depth and RNA composition (7). Second, to scale the normalized count data for linear modelling, the counts were transformed into log2 counts per million and assigned proper weights using the voom method in the limma package (8). Third, technical effects related to differences in library preparation were removed using ComBat from the sva package (9).

A hypoxia signature was computed with a Gene Set Enrichment Analysis (10) using the expression of 42 hypoxia-related genes as reported by Ye et al. (11).

Breast parenchymal density. Breast parenchymal density was assessed according to the ACR BI-RADS Atlas on mammograms acquired at the time of assessment (12).

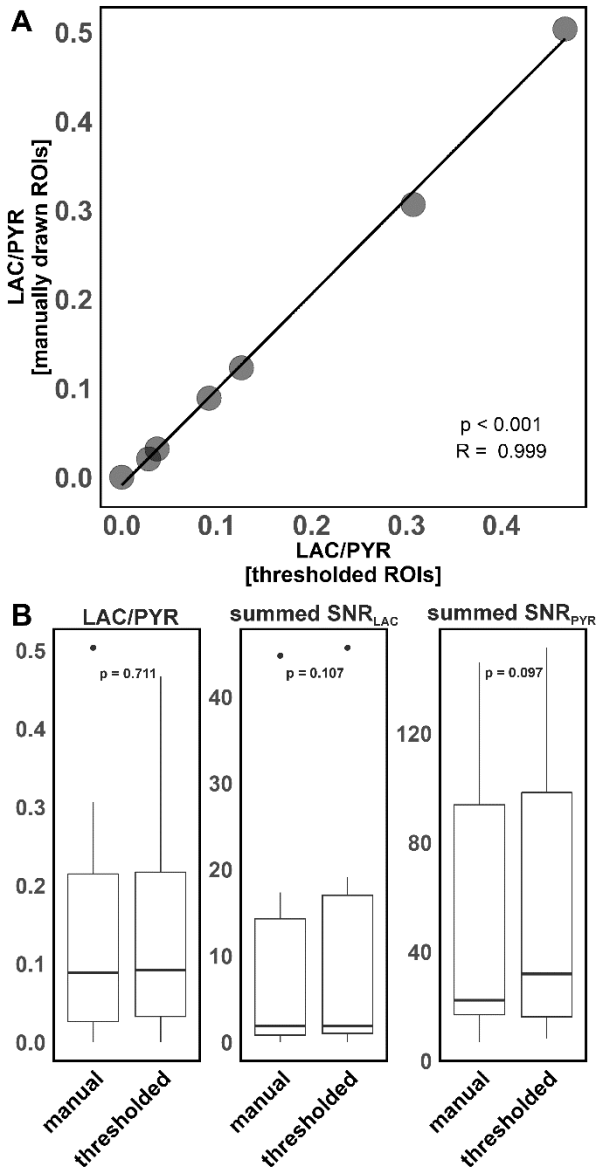

Fig. S1. Relationship between LAC/PYR ratios based on manually drawn versus thresholded ROIs. No significant differences between ROIs drawn in a semi-automated fashion and those drawn manually were found for LAC/PYR ($p = 0.711$), summed SNR_{LAC} ($p = 0.107$) and summed SNR_{PYR} ($p = 0.097$). Center line, median; box limits, upper and lower quartiles; whiskers, 1.5x interquartile range; points, outliers.

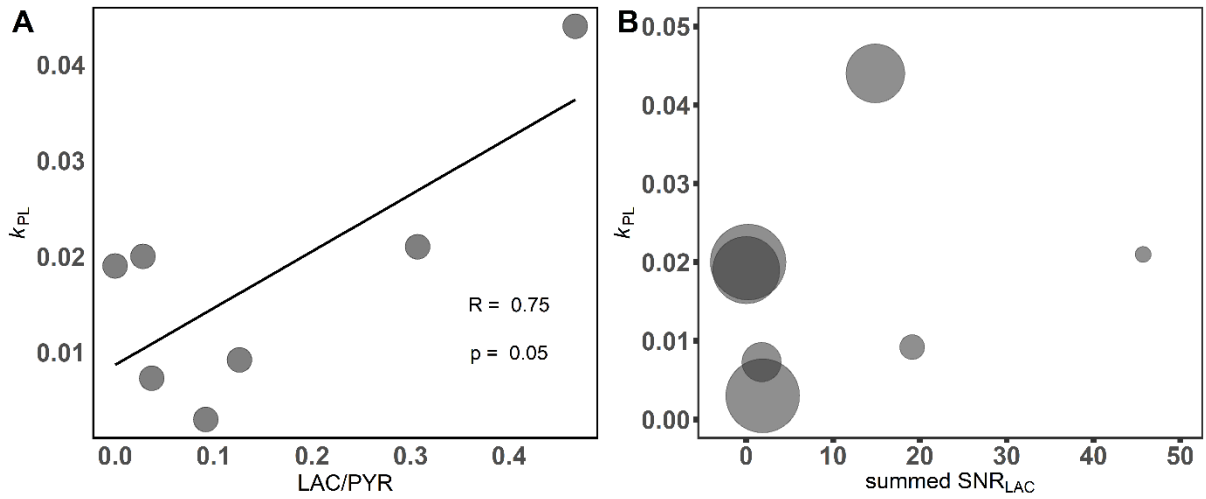

Fig. S2. Relationship between k_{PL}, the LAC/PYR ratio and summed SNR_{LAC}. (A) k_{PL} is significantly correlated with the LAC/PYR ratio. The size of the dot in (B) represents the variance between the measured and fitted time courses for pyruvate and lactate used to estimate k_{PL} (range: 0.012 - 0.66). Tumors with low summed SNR_{LAC} showed the highest variance in k_{PL}.

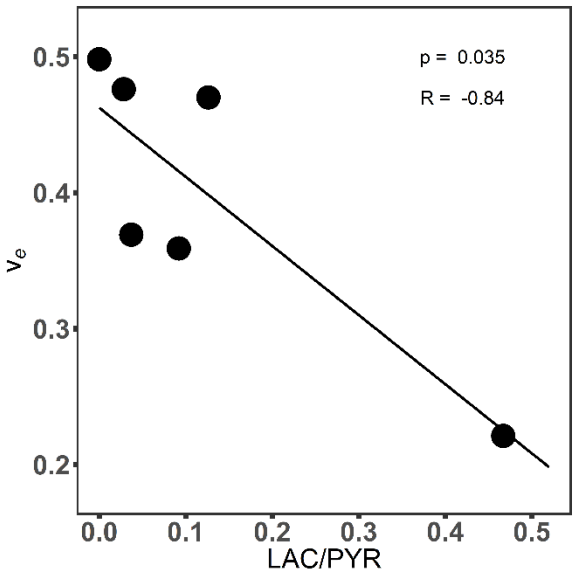

Fig. S3 Relationship between v_e and LAC/PYR. v_e correlated significantly with LAC/PYR but relied heavily on a single outlier.

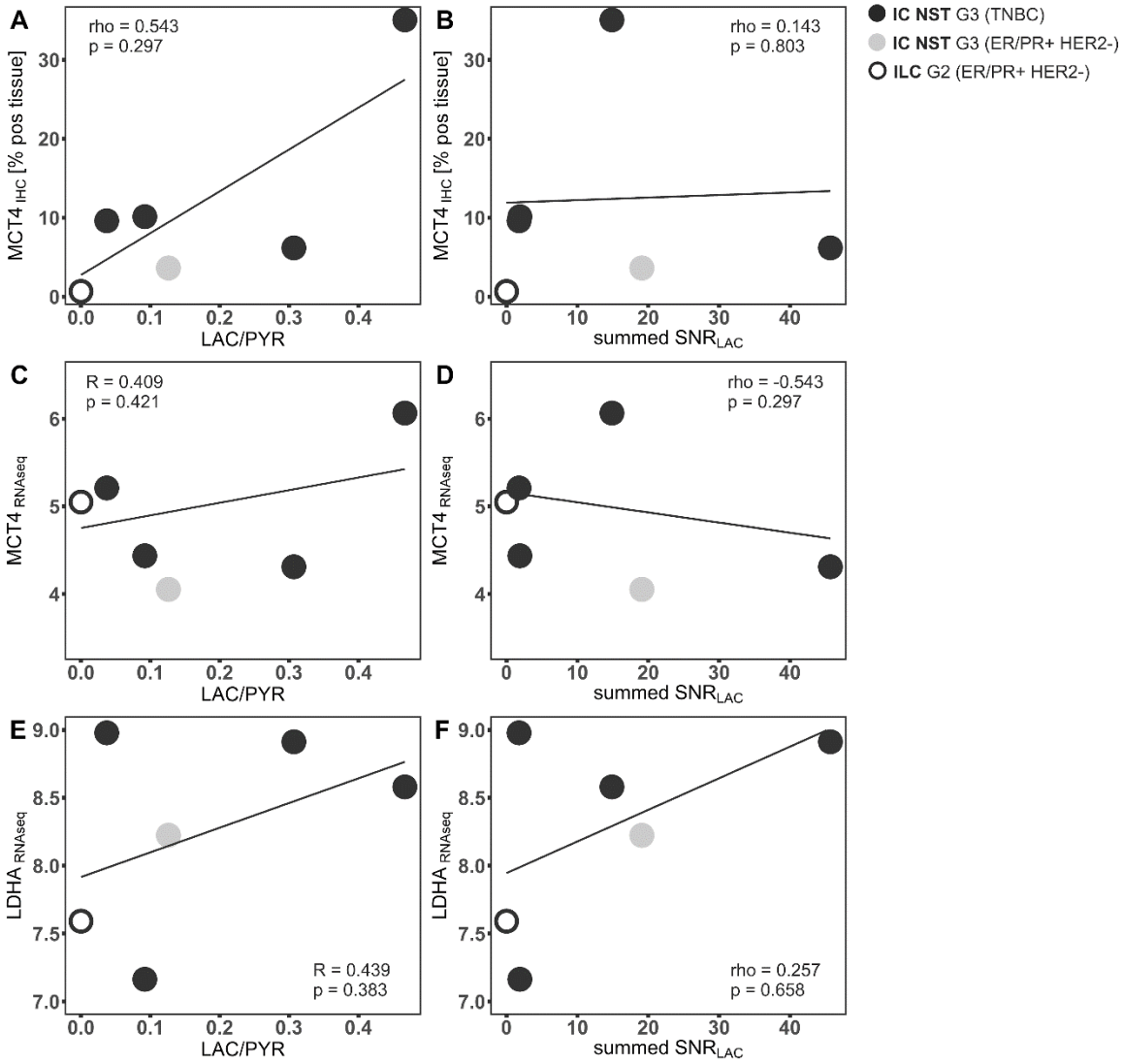

Figure S4. Relationship between hyperpolarized ^{13}C-MRI data (LAC/PYR ratio and summed SNR_{LAC}) and expression of the monocarboxylate transporter4 (MCT4) and lactate dehydrogenase A (LDHA). Correlation of the LAC/PYR ratio and summed SNR_{LAC} with expression of MCT4 assessed by immunohistochemistry and RNA sequencing (A-D). Correlation of the LAC/PYR ratio and summed SNR_{LAC} with expression of LDHA determined by RNA sequencing (E-F).

Table S1 Sequence parameters for IDEAL spiral CSI.

Temporal resolution	2-4 s (2 s in one patient, 4 s in the remaining six patients)
Repetition time (TR)	0.26-0.5 s
Nominal flip angle (FA)	10-15°
Acquisition matrix	40x40
Field of view (FOV)	200-240 mm
Nominal in-plane voxel size	5 x 5 – 6 x 6 mm^2
Reconstructed in-plane voxel size	1.563 x 1.563 -1.875 x 1.875 mm^2
Slice thickness	30 mm
Echo Times (TE)	1.5, 2.7, 3.8, 4.9, 6.0, 7.2, 8.3 ms
RF pulse bandwidth	2289 Hz
Acquisition bandwidth	62500 Hz
Total imaging time	60 s

Table S2 Patient characteristics

Tumor type	Age	BMI	Breast density	Menopausal status	Day of menstrual cycle
IC NST G3 TNBC	62	40.0	scattered FGT	postmenopausal	-
IC NST G3 ER+/PR+/HER2-	76	30.7	heterogeneously dense	postmenopausal	-
ILC G2 ER+/PR+/HER2-	62	32.8	scattered FGT	postmenopausal	-
IC NST G3 TNBC	49	31.1	heterogeneously dense	premenopausal	19
IC NST G3 TNBC	69	21.1	heterogeneously dense	postmenopausal	-
IC NST G3 TNBC	63	30.2	scattered FGT	postmenopausal	-
IC NST G2 ER+/PR+/HER2-	72	28.4	heterogeneously dense	postmenopausal	-

Abbreviations: IC NST, invasive carcinoma no specific type; ILC, invasive lobular carcinoma; G3, grade 3; G2, grade 2; TNBC, triple negative breast cancer; ER, estrogen receptor; PR, progesterone receptor; HER2, HER2/neu; FGT, fibroglandular tissue.

References

1. R. Bedair, *et al.*, Effect of Radiofrequency Transmit Field Correction on Quantitative Dynamic Contrast-enhanced MR Imaging of the Breast at 3.0 T. *Radiology*, 150920 (2015).
2. L. I. Sacolick, F. Wiesinger, I. Hancu, M. W. Vogel, B1 mapping by Bloch-Siegert shift. *Magn Reson Med* **63**, 1315–1322 (2010).
3. F. Zaccagna, *et al.*, Hyperpolarized carbon-13 magnetic resonance spectroscopic imaging: A clinical tool for studying tumour metabolism. *Br. J. Radiol.* **91** (2018).
4. J. T. Grist, *et al.*, Quantifying normal human brain metabolism using hyperpolarized [1–^{13}C]pyruvate and magnetic resonance imaging. *Neuroimage* **189**, 171–179 (2019).
5. C. J. Daniels, *et al.*, A comparison of quantitative methods for clinical imaging with hyperpolarized ^{13}C-pyruvate. *NMR Biomed.* **29**, 387–399 (2016).
6. R. Patro, G. Duggal, M. I. Love, R. A. Irizarry, C. Kingsford, Salmon provides fast and bias-aware quantification of transcript expression. *Nat. Methods* **14**, 417–419 (2017).
7. M. D. Robinson, D. J. McCarthy, G. K. Smyth, edgeR: a Bioconductor package for differential expression analysis of digital gene expression data. *Bioinformatics* **26**, 139–40 (2010).
8. M. E. Ritchie, *et al.*, limma powers differential expression analyses for RNA-sequencing and microarray studies. *Nucleic Acids Res.* **43**, e47 (2015).
9. J. T. Leek, svaseq: removing batch effects and other unwanted noise from sequencing data. *Nucleic Acids Res.* **42**, e161–e161 (2014).
10. A. Subramanian, *et al.*, Gene set enrichment analysis: a knowledge-based approach for interpreting genome-wide expression profiles. *Proc. Natl. Acad. Sci. U. S. A.* **102**, 15545–50 (2005).
11. I. C. Ye, *et al.*, Molecular Portrait of Hypoxia in Breast Cancer: A Prognostic Signature and Novel HIF-Regulated Genes. *Mol. Cancer Res.* **16**, 1889–1901 (2018).
12. V. A. Reston, *The American College of Radiology (ACR) (2013) Breast Imaging Reporting and Data System Atlas (BI-RADS® Atlas)* (2013).